

Mixtures of selected n-alkanes and Au nanoparticles for optical fiber threshold temperature transducers

N. Przybysz^a, P. Marć^a , E. Tomaszewska^b, J. Grobelny^b , L. R. Jaroszewicz^a 

^a Advanced Technologies and Chemistry Faculty, Military University of Technology, 2 Kaliskiego St., 00-908 Warsaw, Poland.

^b Department of Materials Technology and Chemistry, Faculty of Chemistry, University of Lodz, 163 Pomorska St., 90-236 Lodz, Poland.

Article info

Article history:

Received 30 Oct. 2020

Received in revised form 10 Dec. 2020

Accepted 11 Dec. 2020

Keywords:

optical fiber sensors, temperature threshold sensors, gold nanoparticles, n-alkanes, photonic crystal transducers.

Abstract

Thermo-optic properties enhancement of the bi-stable temperature threshold sensors based on a partially filled photonic crystal fiber was reported. Previously tested transducers filled with a selected group of pure n-alkanes had in most cases differences between switching ON and OFF states. Therefore, the modification of filling material by using additional crystallization centers in the form of gold nanoparticles was applied to minimize this undesirable effect. The evaluation of the thermodynamic properties of pentadecane and its mixtures with 14 nm spherical Au nanoparticles based on the differential scanning calorimetry measurements was presented. Optical properties analysis of sensors prepared with these mixtures has shown that they are bounded with refractive index changes of the filling material. Particular sensor switches ON before melting process begins and switches OFF before crystallization starts. Admixing next group of n-alkanes with these nanoparticles allows to design six sensors transducers which change ON and OFF states at the same temperature. Thus, the transducers with a wider temperature range for fiber-optic multi-threshold temperature sensor tests will be used.

1. Introduction

Possibility to use an infiltrated photonic crystal fiber (PCF) in the optical fiber sensor technology was found at an early stage of its development. The most important advantage of infiltrated PCFs is a direct influence on light guided in the fiber with a relatively small amount of the filling material. Such hybrid design has led to various applications. The comprehensive review of applied materials, physical effects and implementations in sensors technology can be found in Refs. 1 and 2. However, from the point of view reported in the paper research, it is worth to mention the studies focused on infiltrated PCF thermo-optic properties. One of the most important physical effects observed in filled PCFs is a change of propagation properties when a refractive index of the filling material decreases with an increase of temperature. This effect was observed in solid and hollow core PCFs when they were

infiltrated by immersing oils [3,4], liquid crystals [5,6,7], phase changing materials [8-11], nanomaterials mixtures, or nano-composites [12-17], and polymers [18,19]. Based on such PCF transducers, various sensors platforms were developed for measurement of different physical parameters [1,2]. Moreover, some special designs were focused on nonlinear optics applications such as dispersion management or supercontinuum generation [20,21].

In this paper, thermo-optic properties of the optical fiber transducers based on a partially filled PCF with the phase transition materials were reported. n-Alkanes from a selected group, used as the filling materials, change their state from solid to liquid for specific temperatures. Phase transition is a discontinuous process and the refractive indices of these materials change discontinuously, as well. These optical properties in connection with optical properties of PCF allow to design a bi-stable optical fiber transducer [8-11] and a multi-stage temperature threshold sensor [10]. Light is able to propagate through such structure when a filling material is in a liquid state – ON state and it stops when a filling material is in a solid state – OFF state. Similar bi-stable effect was demonstrated when

*corresponding author at: pawel.marc@wat.edu.pl

selected n-alkane or paraffin wax were used as a cladding of the tapered optical fiber [22,23].

The unstable thermodynamic properties of n-alkanes or broader paraffins are the critical point in work of such type of bi-stable PCF transducers. For most of these materials, the melting and freezing temperatures are different. This induces a discrepancy between switching ON and OFF temperatures of the transducer. As a solution to this problem, the use of a mixture of pure n-alkanes and metallic nanoparticles was proposed [17]. Nanomaterials are extensively studied in various scientific fields [24]. Enhancement of selected materials optical properties by nanoparticles doping is one of the most interesting subjects of those broad range studies [12,17].

In the paper, gold nanoparticles (Au NPs) were mixed with selected n-alkanes to verify their influence on optical properties of the PCF transducer.

2. Thermodynamic properties of filling materials

2.1. Thermodynamics of n-alkanes phase transition

In the paper the subgroup of n-alkanes with more than 10 carbon atoms in the molecule was taken under consideration due to their melting points which are within the range of $-30-65\text{ }^\circ\text{C}$ and, therefore, they are appropriate to design a bi-stable PCF transducer. Moreover, their physical properties, such as density, melting or boiling point change regularly as the number of hydrocarbon groups in the molecule increases (homologous series). However, they are thermodynamically unstable which is visible as a difference between melting and freezing temperatures when the material changes its phase by its heating or cooling. These thermodynamic properties are directly related to the excess of the system internal energy which results from their internal structure, i.e., a large number of grain boundaries and interphase boundaries. According to Gibbs theory, the undergoing changes are divided into type I or II and each of them is thermally activated [25]. This is due to the fact, that at a temperature lower than the phase transition temperature, the transformation rate is negligible and increases when the diffusion rate is relatively high. In transformation of type I, the energy barrier is triggered by an emergence of a permanent new phase nucleus. This new structure grows in a changed order and has lower energy. In type II, a gradual change of the unstable phase to the stable one occurs through the sequence of intermediate states causing a reduction of material free energy. This type of transformation occurs simultaneously in the entire volume of the material. Change of Gibbs free energy ΔG from the initial to the final state which occurs at the given temperature T is directly related to the changes of enthalpy ΔH and entropy ΔS by the following equation [25]:

$$\Delta G = \Delta H - T\Delta S. \quad (1)$$

Chemical reactions carried out under constant pressure and temperature occur spontaneously if their ΔG is negative. A given system always tends to achieve the minimum of energy in which the further energy reduction is impossible, and, then ΔG reaches a value equal to zero,

i.e., equilibrium. Analyzing the phase transition from liquid to solid, a disordered state of molecules tends to the structure in which each of molecules has a specific location in the crystal lattice. This is type I transformation related to a discontinuous change in entropy which causes a non-linear change in the temperature gradient of ΔG . In this process the latent heat ΔH_f is released at the crystallization point.

In order to initiate a phase transformation, a new phase must be created. Size of a new phase granular structure determines the speed of this transformation. The new phase volume is directly related to the reduction of free energy of the system which is a difference of free energy for the solid and liquid phases (below the melting point). This negative change in free energy per volume should be proportional to the molecule volume. In addition, the nucleation process depends on the solid-liquid interfacial energy γ_{SL} which is associated with an increase in free energy of the system in proportion to the interface surface [25]. A total change of ΔG caused by the generation of a spherical nucleus which has the Gibbs free energy per unit volume ΔG_V and the radius r when the nucleation was assumed is described by the relationship [25]:

$$\Delta G = \frac{4}{3}\pi r^3 \Delta G_V + 4\pi r^2 \gamma_{SL}. \quad (2)$$

In Fig. 1, changes of ΔG_V of the material without modification as a function of temperature were shown.

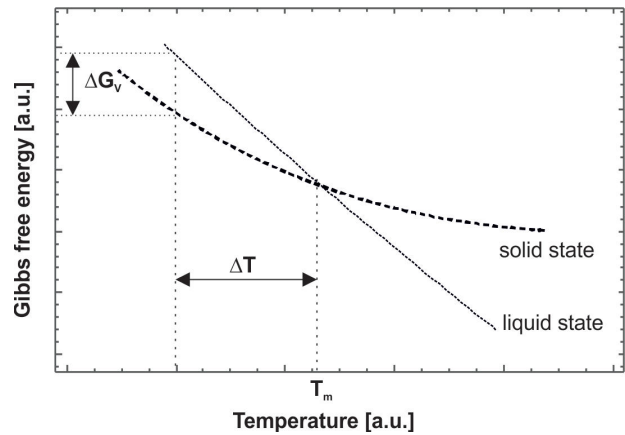


Fig. 1. Graph illustrating the change of Gibbs free energy as a function of temperature near the melting temperature T_m . For subcooling ΔT , the change in free energy per unit volume due to a conversion from liquid to solid is ΔG_V .

At melting point, Gibbs free energy is the same for the liquid and solid states. The solid state of the material is thermodynamically stable below T_m whereas the liquid phase – above it. For temperatures below melting point, Gibbs energy of both states increases. This increase results in an increase of crystallization driving forces. Therefore, a sufficiently large change of ΔG_V of the system is a driving force of the nucleation process and increase in the stability of the base material solid phase.

Equation (2) allows to determine a critical radius of the nucleus r^* [25]:

$$r^* = \frac{2\gamma_{SL}}{\Delta G_V}. \quad (3)$$

If the radius of the admixture nucleus introduced into the base material is smaller than the critical one, then thermodynamic fluctuations of the spherical cluster are unstable, and its growth increases a total free energy of the system. However, if the synthesized nucleus has a size equal or larger than the critical radius, it will be stable, and its increase will reduce the system energy. The latter can lead to reduce the hysteresis between the heating and cooling process. Critical free energy (ΔG_V^*) necessary for the formation of a stable nucleus is determined by the relationship [25]:

$$\Delta G_V^* = \frac{16\pi\gamma_{SL}^3}{3(\Delta G_V)^2} \quad (4)$$

In addition, for slight undercooling ΔG_V can be expressed as the temperature difference ΔT of the melting process related to the melting temperature T_m and determined from equation [25]:

$$\Delta G_V = \frac{L_V}{T_m} \Delta T, \quad (5)$$

where L_V is the latent heat ΔH per unit volume.

Moreover, the above relations indicate that the critical nucleus radius and the nucleation energy barrier are reduced if super-cooling occurs and, thus, the nucleation process is more preferred. However, it is worth to temperature changes. Thermal fluctuations are accompanied by an increase in a local free energy related to ΔG_V^* and the probability of this process depends on the Boltzmann coefficient $\exp(-\Delta G_V^*/kT)$. In addition, the presence of solid phase molecules or particles in a supercooled liquid has a positive effect on the activation energy decrease which is necessary to initiate the crystalline material nucleation process. This is significant because these molecules become preferred nucleation centers. When analyzing the heterogeneous nucleation, the critical activation energy of the nucleation process is reduced by a geometric factor that specifies the nucleus efficiency by the contact angle (θ) and is presented as [25]:

$$f(\theta) = \frac{1}{4}(1 - \cos \theta)^2(2 + \cos \theta). \quad (6)$$

Hence, ΔG^* is written as follows [26]:

$$\Delta G^* = \frac{16\pi\gamma_{SL}^3 T_m^2}{3L_V^2} \frac{1}{\Delta T^2} f(\theta). \quad (7)$$

Contact angle less than π significantly reduces the undercooling degree. The preferred and effective nucleation center is the given phase existing nucleus and then the contact angle is zero [25].

2.2. Thermodynamic properties of selected n-alkanes and their Au nanoparticles mixtures

In previous experiments, switching ON and OFF temperatures of the tested PCF transducers were different when they were heated and cooled [10]. Thermodynamic considerations presented in the previous paragraph allow to understand how to design a proper filling material of

transducers based on selected n-alkanes. Therefore, the main aim of this work is to find a possibility to compensate an undesirable temperature effect by using alkali tightly dedicated nanoparticles (NPs) as an admixture. Appropriately designed shape, size, and chemical composition on the surface of the NPs to prevent unwanted agglomerations were considered.

Gold (Au) NPs transferred from an organic colloid as an admixture of selected n-alkanes act as nucleation centers and increase a thermodynamic stability of the system. It was expected that this effect reduces the observed hysteresis between switching ON and OFF temperatures while the PCF transducer is heated and cooled.

In the higher alkanes selection process, the melting temperature and the refractive index were taken into consideration. Melting temperatures of alkanes were different of around 10 °C and always less than 70 °C. The refractive index of the material in a liquid state was lower than the refractive index of silica.

As a modifier of n-alkane Au NPs were used. They were prepared as a stabile colloid of Au NPs uniformly dispersed in an organic solvent without agglomeration effect. Preparation of Au NPs colloids was a two-stage experiment which was partially described in the previous work [17]. Briefly, in the first stage, the synthesis of Au NPs was performed by a chemical reduction method in an aqueous solution. For this purpose, a gold precursor solution (HAuCl₄) of an appropriate concentration was prepared and heated to the boiling point under reflux. Then, a heated reductant solution was vigorously introduced which also acted as a stabilizer. Table 1 presents the list of reagents used for the synthesis.

Table 1
List of reagents used for Au NPs synthesis in a size of 5 nm and 14 nm.

Sizes of Au NPs	5 nm	14 nm	
Concentration of Au	100 ppm	100 ppm	
Molar ratio of HAuCl ₄ :sodium citrate:tannic acid	1:3:2	1:3.5:0	
Gold precursor HAuCl ₄	94.34 g, 0.0183%	95.42 g, 0.0181%	
Reductant solution	Sodium citrate	3.93 g, 1%	4.58 g, 1%
	Tannic acid	1.73 g, 1%	-

After the reductant was added, the solution turned red which proves the formation of gold nanoparticles (after 1 min for 14 nm Au NPs and immediately for 5 nm Au NPs). The solution was stirred for additional 15 min and next cooled down to room temperature. The next stage of the Au NPs colloid synthesis was based on the phase transfer process. In order to obtain Au NPs organic colloids, octadecylamine was used as a modifier. Alkylamines with long hydrophobic chains were selected as Au NPs surface modifiers. Selected modifiers enabled the transfer of Au NPs suspended in water to hexane and obtaining stable organic colloid systems. The modifier amount corresponds to 50 molecules of octadecylamine per

1 nm^2 of an NPs surface. To fully replace the ligand already adsorbed on the NPs surface (citrate) in water and enable a phase transfer, an excess of incoming ligand (amine) should be provided. The weight ratio of aqueous colloid to hexane was 1:1, thus the Au mass concentration did not change and was of 100 ppm. The bi-phasic system was shaken for 5 min and then left for another 2 min. Subsequently, the system spontaneously separated into two layers, hexane phase and water phase.

The obtained Au NPs were examined using the scanning transmission electron microscopy (STEM) technique to give complementary information about size, size distribution and shape of nanoparticles (Fig. 2). The aqueous and organic Au NPs colloids were characterized using a dynamic light scattering (DLS). As a result, the hydrodynamic diameter of the obtained Au NPs was determined and the effective phase transfer process was confirmed (Fig. 3).

As shown in Fig. 2, the obtained nanoparticles are monodispersed and quasi-spherical. In order to obtain a size distribution histogram, 500 particles were measured and the mean Au NPs size was determined as $5 \pm 1 \text{ nm}$ and $14 \pm 2 \text{ nm}$, respectively.

As shown in Fig. 3(a), differences in size obtained by two techniques (DLS and STEM) are related to the measured value specificity. In the DLS technique, hydrodynamic diameters of nanoparticles (metallic cores together with modifiers/stabilizers adsorbed on the surface)

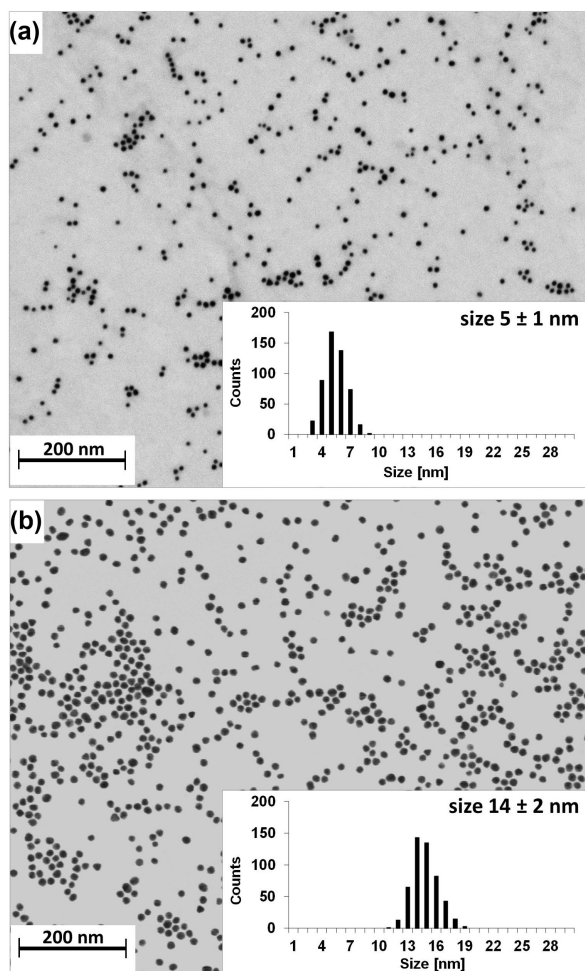


Fig. 2. STEM images with corresponding particle size distributions histograms of Au NPs: measured size (a) $5 \pm 1 \text{ nm}$; (b) $14 \pm 2 \text{ nm}$.

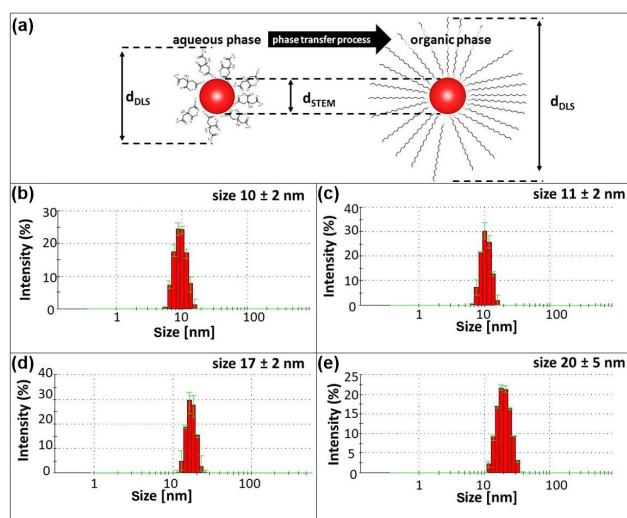


Fig. 3. Schematic presentation of the measured size in DLS and STEM techniques (a); DLS size distribution graphs of Au NPs 5 nm – measured hydrodynamic diameters were $10 \pm 2 \text{ nm}$ in aqueous phase (b) and $11 \pm 2 \text{ nm}$ in hexane phase (c); DLS size distribution graphs of Au NPs 14 nm – measured hydrodynamic diameters were $17 \pm 2 \text{ nm}$ in aqueous phase (d) and $20 \pm 5 \text{ nm}$ in hexane phase (e).

are measured, and, therefore, larger sizes are obtained, while in the STEM technique only diameters of metallic cores are measured. Thus, the nanoparticles size obtained by the STEM technique compared with DLS will be smaller. In order to confirm the effectiveness of the phase transfer process, measurements of the hydrodynamic diameter were performed using the DLS technique. The measured hydrodynamic diameter for 5 nm Au NPs (STEM) in water was $10 \pm 2 \text{ nm}$ [Fig. 3(b)] and $11 \pm 2 \text{ nm}$ in hexane phase [Fig. 3(c)]. The measured hydrodynamic diameter for 14 nm Au NPs (STEM) in water was $17 \pm 2 \text{ nm}$ [Fig. 3(d)] and $20 \pm 5 \text{ nm}$ in hexane phase [Fig. 3(e)]. No aggregates or agglomerates were detected after the phase transfer process.

In general, a mixture of n-alkane and Au NPs colloid was prepared according to the following procedure. 1 ml of a higher alkane and 1 ml of a colloid with Au NPs were mixed in one glass phial. This was a composition of 1:1. The 1:x composition has x ml of Au NPs colloid. Next, the mixture was intensively mixed and heated at a temperature higher than the evaporation temperature of a colloid solvent at which the NPs were stabilized. After the solvent evaporation, the mixture was checked whether the resulting material had undesirable effects such as splitting into two phases or agglomerates. If any negative effect was observed, the mixture was ready to make a PCF transducer.

In the research, two sizes of Au NPs in a colloid were tested. PCF transducers based on mixtures with 5 nm Au NPs and selected higher alkanes had adverse effects and an increase of switching ON and OFF temperatures was observed. Regarding Eq. (3), it could be a result of a smaller than critical radius of the nucleus. Thus, the prepared mixtures were thermodynamically unstable. In the next step, 14 nm Au NPs were tested. However, before the PCF transducers preparation, influence on thermodynamic properties of n-alkane by Au NPs was verified by differential scanning calorimetry (DSC) measurements [26]. In the experiments, mixtures compositions of

n-alkane/Au NPs colloid in the following proportion: 1:x where $x=0.6$ were prepared. DSC measurements were made using the Netzsh DSC 204 F1 Phoenix calorimeter. Studies were conducted in the ambient atmosphere of nitrogen with a gas flow rate of 20.0 ml/min and a heating/cooling rate of 2.0 °C/min.

As examples, see Fig. 4, DSC measurements of pure pentadecane ($C = 15$) and its first two mixtures were used.

In all presented plots, blue and red curves represent a heat flow per unit sample vs. temperature for cooling and heating processes, respectively. For higher concentrations, both crystallization and melting temperatures remain unchanged. During the heating process the tested material is in a solid phase. Heat transport mechanism is based on

conduction and a much larger temperature gradient is observed in the system. Each plot consists of two peaks which are related to increased temperatures of solid-solid [26] and solid-liquid transitions. When a mixture is cooled, only a liquid phase is present in the initial stage and the heat exchanged between the environment and the mixture is relatively high. Phase transitions from liquid to solid and next solid-solid are represented as depths on these plots. Each peak/depth is described by a set of data which are: area and onset, peak and end temperatures.

Onset and end temperatures allow to calculate ΔT from Eqs. (5) and (7). Peak temperature which indicates crystallization (T_c) or melting (T_m) temperature defines the meta-stable zone width $T_{MSZW} = T_m - T_c$ [27]. Therefore, to simplify the analysis of solid-liquid-solid transitions when the sample is heated or cooled, in Table 2 cumulative data of peaks temperatures of the tested pentadecane for all prepared concentrations were shown.

Table 2

Crystallization and melting temperatures, meta-stable zone width and latent heat of solid-liquid-solid phase transitions based on DSC measurements for pentadecane and its mixtures

Mixture composition	1:0	1:1	1:2	1:3	1:4	1:5	1:6
T_c [°C]	6.4	6.6	7.0	7.1	7.0	7.0	7.0
L_v [J/g]	153.4	151.4	151.0	146.8	150.1	148.5	148.5
T_m [°C]	13.2	12.8	12.5	12.4	12.4	12.4	12.4
L_{vm} [J/g]	149.2	146.4	146.8	143.5	145.7	144.0	144.0
T_{MSZW} [°C]	6.8	6.2	5.5	5.3	5.4	5.4	5.4

L_v, L_{vm} denote latent heats of crystallization and melting processes, respectively.

Melting temperatures in the heating process are within the range of 12.4–13.2 °C, while crystallization transition temperatures of the cooling process for all examined cases are between 6.4 °C and 7.1 °C. The data show that the transfer of Au NPs to the pentadecane allows to reduce T_{MSZW} of about 1.5 °C because of a simultaneous decrease of T_m and an increase of T_c . Significant changes in the above-mentioned temperatures took place already at the lowest concentrations of NPs, i.e., 1:1 and 1:2. The influence of higher NPs concentrations was within the uncertainty limit.

In a phase transition point the free Gibbs energy change ($\Delta G_{p.t.}$) equals 0. Therefore, from Eq. (1) it is possible to calculate entropy ($\Delta S_{p.t.}$) which is enthalpy ($\Delta H_{p.t.}$) and peak temperature (ΔT_{peak}) ratio. These values are shown in the DSC thermograms as the insets in Fig. 4. In Table 3 summarized calculations for the pure pentadecane and its Au NPs 1:1 and 1:2 mixtures for the heating and cooling processes are shown. The admixture in the form of NPs slightly decreases both $\Delta H_{p.t.}$ and $\Delta S_{p.t.}$ during the liquid-solid and solid-solid phase transition compared to the pure n-alkanes. The latent heat L_v decreases as the mass fraction of gold nanoparticles increases. L_v is attributed to the intermolecular van der Waals forces and to ordering the n-alkane structure by introducing additional crystallization centers. The limited thermal translational movements of individual alkane molecules by arranging the mixture with nanoparticles reduce L_v and change ΔS , as well. Moreover, with an increase of NPs concentration latent heats of both melting

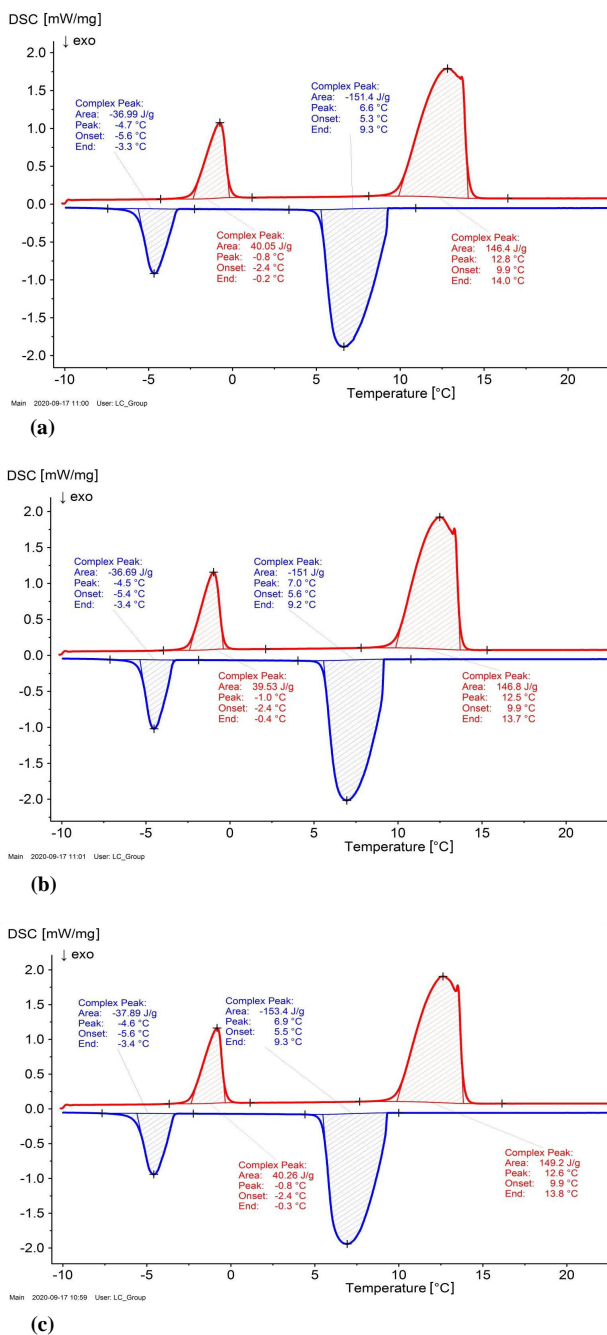


Fig. 4. DSC measurements of pentadecane and its Au NPs mixtures with the following proportions of n-alkane and Au NPs colloid: (a) 1:0, (b) 1:1, (c) 1:2. Red color indicates heating while blue one indicates the cooling process.

L_{Vm} and crystallization L_{Vc} processes decrease and less energy is necessary to transform the prepared mixture from one phase to another. Area is related to the integral of the plot between onset and end temperatures and is the L_V value of the phase transformation [Eq. (5)].

Table 3.

Calculated entropy ($\Delta S_{p.t.}$) changes based on DSC measurements for heating and cooling of pure pentadecane and its Au NPs mixtures for concentrations of 1:1 and 1:2.

Mixture composition	$\Delta H_{p.t.}$ [kJ/mol]	T_{peak} [K]	$\Delta S_{p.t.}$ [J/mol·K]	
Heating	1:0	31.69	285.75	110.91
		8.55	272.35	31.40
	1:1	31.10	285.95	108.75
		8.51	272.35	31.24
	1:2	31.18	285.65	109.16
		8.40	272.15	30.85
Cooling	1:0	-32.58	280.05	-116.35
		-8.05	268.55	-29.97
	1:1	-32.16	279.75	-114.96
		-7.86	268.45	-29.27
	1:2	-32.07	280.15	-114.49
		-7.79	268.65	-29.01

3. Optical properties of PCF transducers

In the next step of the research, a set of PCF transducers based on synthesized mixtures with 14 nm Au NPs was prepared. The manufacturing procedure was as follows. In the first stage, after the base material modification (higher alkane), it was introduced into the air holes of a PCF by means of capillary forces, at elevated temperature and pressure. Next, the material was moved to an appropriate distance from the optical fiber end by using external vacuum. Finally, standard telecommunication fibers with FC APC connectors were spliced to both ends of the partially filled PCF. In the experiment an LMA 10 PCF (ThorLabs) with a length of about 25 cm was applied. The standard filling length was of around 40 mm. In this configuration each patch cord is a single sensor which works as a bi-stable temperature sensor. When temperature is high enough to melt the filling material and its refractive index is lower than the optical fiber material refractive index, the light can pass through the sensor (state ON). If one of these conditions is not fulfilled, the sensor does not transmit light (state OFF) [10]. Temperature at which the light can pass through the sensor is named T_{ON} , while the temperature at which the light is stopped is named T_{OFF} .

Optical properties measurements of the prepared transducers were carried out in an experimental set-up presented in Fig. 5. In the above set-up it is possible to test four transducers (S1, S2, S3, S4) simultaneously. Light from the laser diode (central wavelength of 850 nm) is divided by a 1x4 uniform splitter and illuminates each sample. Light intensity passing through a single element is measured by a detector. Analog signals from all tested transducers are converted by A/D converters and acquired by PC.

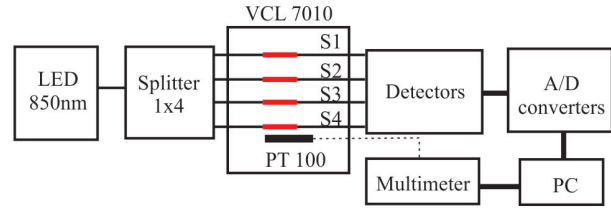


Fig. 5. The experimental set-up for the PCF transducer characterization.

To reduce temperature fluctuation inside the temperature chamber (VCL 7010), all prepared samples were isolated in a single metal tube. Additional information acquired by PC was temperature calculated based on resistance of the PT100 thermocouple placed inside this metal tube. For each transducer, the measured light intensity changes in a specific range of temperature which is around the solid-liquid transition temperatures of the filling material used. Usually two heating – cooling cycles were carried out. Measurement voltages were read from detectors with a speed of 1 S/s.

During each test, the sensor time response was measured. However, to evaluate thermo-optic properties of the transducers, these data were plotted as normalized voltage measured by the photodetector vs. temperature measured by the thermocouple.

As an example of such measurements, in Fig. 6 a normalized voltage of PCF transducers based on pentadecane and its mixtures is presented. The temperature span for all samples was within the range of 0–20 °C. By analogy to Fig. 4, measurements data are marked in red when the sample was heating and in blue when it was cooling.

Optical properties of the pure pentadecane presented in Fig. 6(a) show that it switches OFF (T_{OFF}) and ON (T_{ON}) for temperatures of around 5.4 °C and 7.7 °C, respectively. However, transferred from colloidal, NPs cause fluctuations of ON and OFF temperatures. For a mixture composition of 1:1 [Fig. 6(b)], the presence of NPs results in the shift of both temperatures to lower values and T_{OFF} is of around 3.8 °C while T_{ON} is of around 6.1 °C. Next, a transducer with a 1:2 mixture [Fig. 6(c)] has $T_{OFF} = 7.8$ °C and $T_{ON} = 9.1$ °C. Finally, for a mixture composition of 1:5, both switching temperatures equalize. This mixture composition fulfills requirements of a developed PCF transducer.

Comparing these data with the measured melting and crystallization temperatures presented in Table 2, it is obvious that the optical transmission observed in measurements appears for lower temperatures than filling material changes its phase. When this mixture starts to melt, its refractive index decreases and because its value is lower than silica light, it can pass through the transducer.

Detailed analysis of Fig. 6(a) shows that the heat flow of a pure pentadecane starts to increase of around 8 °C which co-relates with T_{ON} temperature. When the transducer was cooling, the intensity decreased slowly and around T_{ON} dropped indicating the start of the phase transition. Due to a super-cooling effect of the melted material, T_{OFF} is of around 5.4 °C what correlates with an onset temperature of the DSC measurement of the crystallization peak. Unfortunately, the above-mentioned correlation of a pure material is not in coincidence with NPs mixtures.

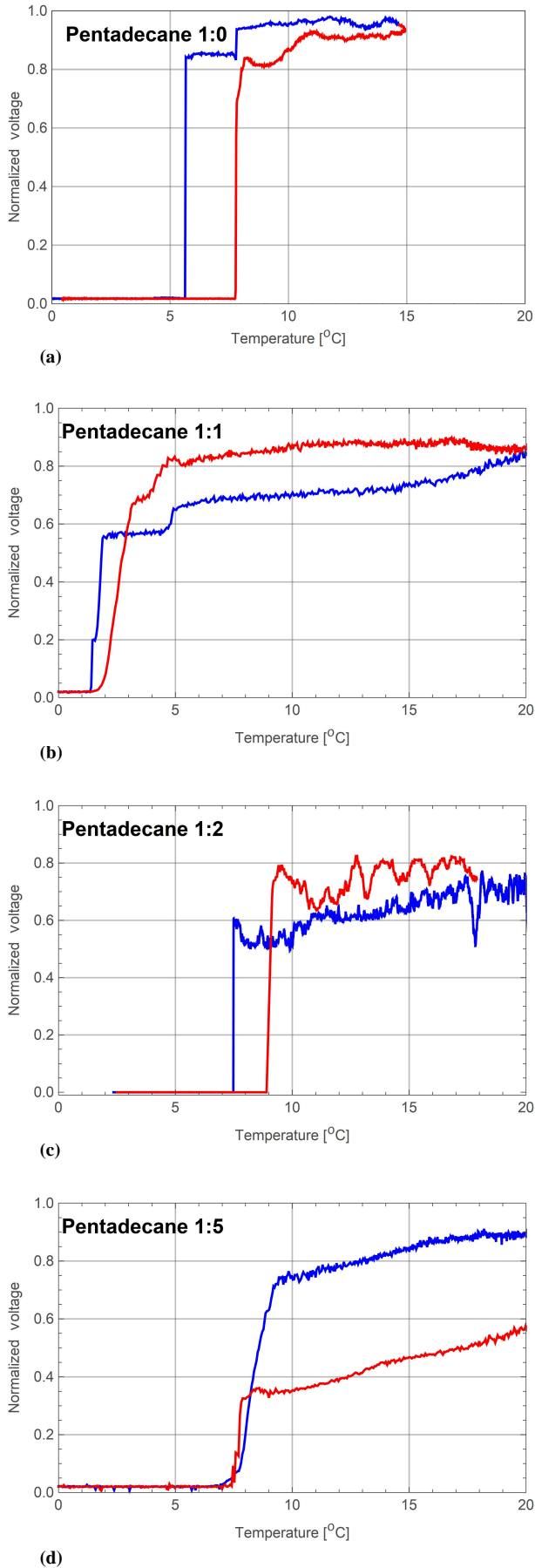


Fig. 6. Temperature responses of PCF transducers based on pentadecane and its Au NPs mixtures in a volume ratio: (a) 1:0, (b) 1:1, (c) 1:2 and (d) 1:5. Red color indicates heating while blue one indicates cooling process.

Therefore, taking into consideration data in Figs. 6(c) and 6(d), the application of Au NPs has increased refractive indices of the mixtures in their liquid state. And the PCF transducer filled with a 1:5 mixture has its refractive index at switching ON and OFF temperature exactly below the refractive index of silica. It is because the filling material refractive index, when phase transition effects are observed, is in the region in which waveguide properties of a filled PCF are shifted to a non-guiding or band gap guiding region [1,2]. Moreover, influence of an optical attenuation increase of a filling material in solid state should be considered.

In further studies, eleven *n*-alkanes with carbon atom numbers between 12 and 28 were tested to verify the suppression possibility of observed discrepancy between T_{ON} and T_{OFF} .

A mixed mixture was prepared with the same composition as for pentadecane. For all tested pure and mixed with Au NPs *n*-alkanes, a bi-stable work of individual transducers was observed and most of them had no zero temperature difference between ON and OFF states.

In Fig. 7 cumulative data of optical properties of PCF transducers based on all tested *n*-alkanes and their mixtures were presented. In the aggregated plots are shown materials with the increased number of carbon atoms from the top to the bottom. Mixture compositions are indicated at the bottom of the plot. In general, for six *n*-alkanes, i.e., tridecane, pentadecane, nonadecane, heneicosane, tetracosane, and octacosane it was possible to find a proper concentration mixture for which T_{ON} and T_{OFF} of a PCF transducer are equal or very close to each other. For hexadecane and heptadecane, it was possible to reduce a difference between these temperatures of around 2 °C when the mixture concentration was of 1:6 and 1:5, respectively. For three materials, i.e., dodecane, tetradecane and octadecane it was impossible to find a proper concentration of Au NPs in the mixture for a sufficient reduction of these temperatures. It is also visible that *n*-alkanes with odd number of carbon atoms allow to design proper optical properties of the transducer. Additionally, with the increase of the carbon atom number, discrepancy between ON and OFF states decreases. Moreover, thermal anomalies observed in some measurements are related to changes of a heating/cooling rate gradient which induces the shift of crystallization and melting temperatures and directly influences optical properties of the tested transducers [27].

4. Conclusions

A previous research concerning thermo-optic effects in bi-stable threshold temperature transducers based on a partially filled PCF had led to the observation of a hysteresis of single sensor ON and OFF states. Temperatures at which a single sensor has switched ON and OFF during heating or cooling processes were usually different. Main reason for that was a thermodynamic instability of the *n*-alkane used. To overcome this phenomenon, the heterogeneous nucleation centers in the form of Au NPs were added to the base material. This additive increased the activation energy of *n*-alkanes and NPs system. In this way the initiation of a crystallization

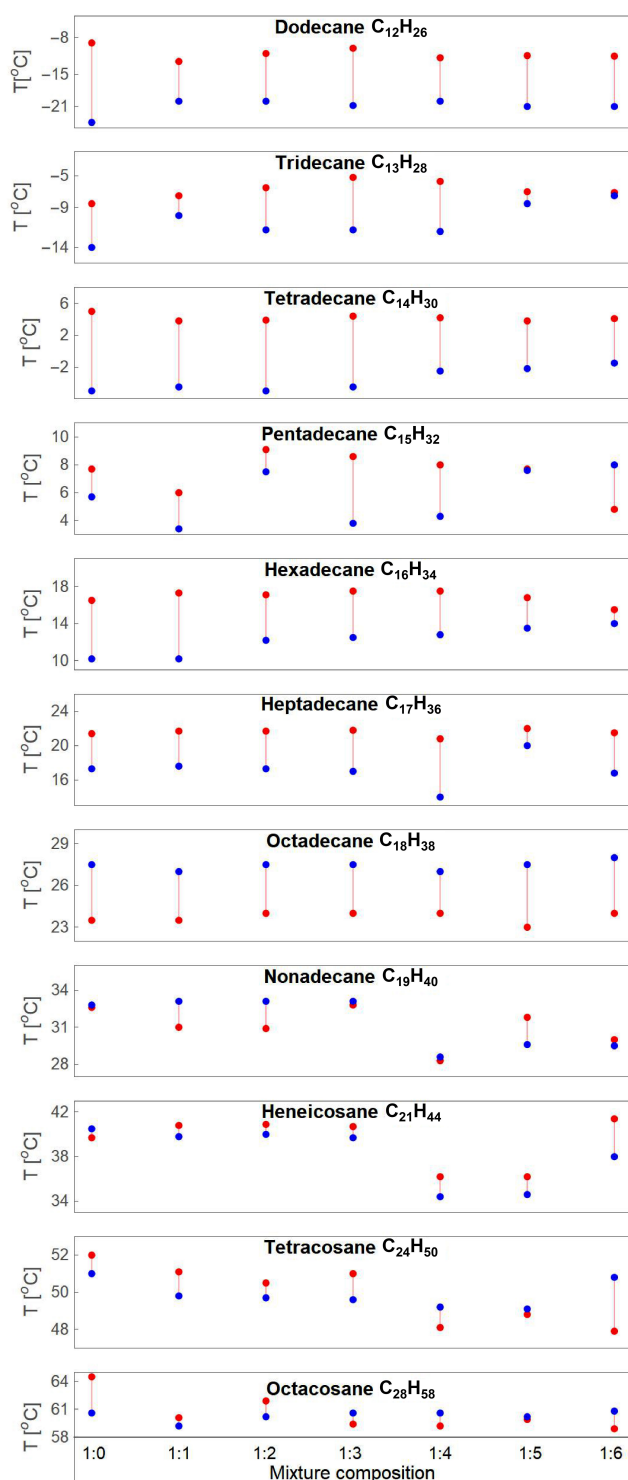


Fig. 7. Switching ON (T_{ON}) and OFF (T_{OFF}) temperature modifications for selected n-alkanes and their Au NPS mixtures with 1:0, 1:1, 1:2, 1:3, 1:4, 1:5, 1:6 mixture compositions. Red color indicates heating while blue one indicates cooling process.

process by this type of nucleus reduced the super-cooling effect observed in this kind of material. Presented thermodynamic considerations were verified by a DSC measurements of pentadecane and its Au NPs mixtures. Two sizes of Au NPs were tested. Au NPs with an average size of 5 nm were too small to stabilize thermodynamics of the selected n-alkanes and the optical properties of the tested PCF transducers were not acceptable. Au NPs with an average size of 14 nm allowed to prepare mixtures

required by a PCF transducer. From the group of 12 selected n-alkanes with the number of carbon atoms higher than 11, in six cases there were found optimal concentrations of NPs to sufficiently reduce switching ON and OFF temperatures. Data analysis shows that the thermodynamic effects caused by the NPs admixture were also accompanied by an increase of the refractive index which contributed to a significant improvement in the parameters of the tested elements. Based on the tested materials, it is possible to select n-alkanes with a proper concentration of Au NPs in the mixture which allows to create a fiber optic multi-stage temperature threshold sensor with a dedicated temperature span.

Authors' statement

Authors' contributions to this paper are as follows: research concept PM, NP, LRJ, experimental study NP, ET, collection and assembly of data, PM, NP, ET, data analysis and interpretation PM, NP, ET, JG, LRJ; writing the article PM, NP, ET, JG, LRJ; critical revision of the article JG, LRJ; final approval of the article PM, NP, ET, JG, LRJ.

Acknowledgements

We acknowledge a very fruitful discussion with Michał Czerwiński, PhD about thermodynamics of n-alkanes and his help with DSC measurements.

This work was financially supported by the Ministry of Science and Higher Education as a statutory activity of Technical Physics Applications Department of the Military University of Technology.

References

- [1] Algorri, J.F. *et al.* Infiltrated Photonic Crystal Fibers for Sensing Applications. *Sensors* **18**, 4263 (2018). <https://doi.org/10.3390/s18124263>
- [2] Markos, Ch. *et al.* Hybrid photonic-crystal fiber. *Rev. Mod. Phys.* **89**, 045003 (2017) <https://doi.org/10.1103/RevModPhys.89.045003>
- [3] Wang, Y. *et al.* Temperature-controlled transformation in fiber types of fluid-filled photonic crystal fibers and applications. *Opt. Lett.* **35** (1), 88–90 (2010). <https://doi.org/10.1364/OL.35.000088>
- [4] Wang, Y. *et al.* Thermo-optic switching effect based on fluid-filled photonic crystal fibre. *IEEE Photonic Tech. L* **22** (3), 164–166 (2010). <https://doi.org/10.1109/LPT.2009.2037242>
- [5] Larsen, T. & Bjarklev, A. Optical devices based on liquid crystal photonic bandgap fibers. *Opt. Express* **11**, 2589–2596 (2003). <https://doi.org/10.1364/OE.11.002589>
- [6] Ertman, S., Rutkowska, K. & Wolinski, T. R. Recent progress in liquid-crystal optical fibers and their applications in photonics. *J. Lightwave Technol.* **37** (11), 2516–2526 (2019). <https://doi.org/10.1109/JLT.2018.2869916>
- [7] Lee, Ch., Wu, Ch., Chem, Ch., Jau, H. & Lin, T. Polarization-independent bistable light valve in blue phase liquid crystal filled photonic crystal fiber. *Appl. Opt.* **52**, 4849–4853 (2013). <https://doi.org/10.1364/AO.52.004849>
- [8] Marć, P., Przybysz, N., Stasiewicz, K. & Jaroszewicz, L. R. Alkanes-filled photonic crystal fibers as sensor transducers. *Proc. SPIE* **9634**, 963450 (2015). <https://doi.org/10.1117/12.2191417>
- [9] Marć, P., Przybysz, N., Stasiewicz, K. & Jaroszewicz, L. R. Multilevel temperature threshold sensor based on Photonic Crystal Fiber transducers. *Proc. SPIE* **10323**, 103231T (2017). <https://doi.org/10.1117/12.2262101>
- [10] Marć, P., Przybysz, N., Molska, A. & Jaroszewicz, L. R. Photonic Crystal Fiber Transducers for an Optical Fiber Multilevel Temperature Threshold Sensor. *J. Lightwave Techn.* **36**, 898–903 (2018). <http://doi.org/10.1109/JLT.2017.2759202>

- [11] Peng, Y., Hou, J., Zhang, H., Xiao, R. & Lu, Q. Temperature sensing using the bandgap-like effect in a selectively liquid-filled photonic crystal fiber. *Opt Lett.* **38**, 263–265 (2013). <https://doi.org/10.1364/OL.38.000263>
- [12] Lesiak, P. et al. Self-Organized, One-Dimensional Periodic Structures in a Gold Nanoparticle-Doped Nematic Liquid Crystal Composite. *ACS Nano* **13**, 10154–10160 (2019). <https://doi.org/10.1021/acsnano.9b03302>
- [13] Marć, P. et al. Thermo – optic properties of Co nanofluid filled microstructured fiber. *Proc. SPIE* **8794**, 87942J (2013). <https://doi.org/10.1117/12.2025233>
- [14] Miao, Y., Liu, B., Zhang, K., Liu, Y. & Zhang, H. Temperature tunability of photonic crystal fibers filled with Fe₃O₄ nanoparticles fluid. *App. Phys. Lett.* **98**, 021103 (2011). <https://doi.org/10.1063/1.3540647>
- [15] Thakur, H. V., Nalawade, S. M., Gupta, S. & Kitture, R. Photonic crystal fiber injected with Fe₃O₄ nanofluid for magnetic field detection. *App. Phys. Lett.* **99**, 161101 (2011). <https://doi.org/10.1063/1.3651490>
- [16] Scolari, L. et al. Frequency tunability of solid-core photonic crystal fibers filled with nanoparticle-doped liquid crystals. *Opt. Express* **17**, 3754–3764 (2009). <https://doi.org/10.1364/OE.17.003754>
- [17] Przybysz, N., Marć, P., Tomaszewska, E., Grobelny J. & Jaroszewicz, L. R. Pure and Au nanoparticles doped higher alkanes for an optical fiber temperature threshold sensor. *Proc. SPIE* **10231**, 1023125 (2017). <https://doi.org/10.1117/12.2265867>
- [18] Westbrook, P.S. et al. Cladding-mode resonances in hybrid polymer-silica microstructured optical fiber gratings. *IEEE Photonic Tech L* **12** (5) 495–497 (2000). <http://doi.org/10.1109/68.841264>
- [19] Balakrishnan, M. et al. Polymer-Filled Silica Fibers as a Step Towards Electro-Optically Tunable Fiber Devices. *J. Lightwave Techn.* **30** (12) 1931–1936 (2010). <https://doi.org/10.1109/LPT.2009.2037242>
- [20] Canh, T. et al. Supercontinuum generation in all-normal dispersion suspended core fiber infiltrated with water. *Opt. Mater. Express* **10**, 1733–1748 (2020). <https://doi.org/10.1364/OME.395936>
- [21] Kim, S. E. et al. Elliptical defected core photonic crystal fiber with high birefringence and negative flattened dispersion. *Opt. Express* **20**, 1385–1391 (2012). <https://doi.org/10.1364/OE.20.001385>
- [22] Stasiewicz, K. & Musiał, J. Threshold temperature optical fiber sensors. *Opt. Fib. Tech.* **32**, 111–118 (2016). <https://doi.org/10.1016/j.yofte.2016.10.009>
- [23] Said, A., Salah, A. & Fattah, G. A. Enhanced Thermo-Optical Switching of Paraffin-Wax Composite Spots under Laser Heating. *Materials* **10** (5), 525 (2017). <https://doi.org/10.3390/ma10050525>
- [24] Jeevanandam, J. et al. Review on nanoparticles and nanostructured materials: history, sources, toxicity and regulations. *Beilstein J Nanotechnol.* **9**, 1050–1074 (2018). <https://doi.org/10.3762/bjnano.9.98>
- [25] Toddin, I. Processing and properties of inorganic nanomaterials. in *Nanoscale Science and Technology* (eds. Kelsall, R., Hamley, I.W. & Geoghegan, M.) 237–245 (John Wiley & Sons, Inc., 2005). <https://doi.org/10.1002/0470020873>
- [26] Taggart, A. M., Voogt, F., Clydesdale, G. & Roberts, K. J. An examination of the nucleation kinetics of n-alkanes in the homologous series C₁₃H₂₈ to C₃₂H₆₆, and their relationship to structural type, associated with crystallization from stagnant melts, *Langmuir* **12**, 5722–5728 (1996). <https://doi.org/10.1021/la9600816>
- [27] Johnson, J. F. Phase Transformations in Commercial Paraffin Waxes. A refractometric study. *Ind. Eng. Chem.* **46**, 1046–1048 (1954). <https://doi.org/10.1021/ie50533a062>